

# Thermodynamic assessment of Co-Al-W system and solidification of Co-enriched ternary alloys

Y. F. Cui · X. Zhang · G. L. Xu · W. J. Zhu ·  
H. S. Liu · Z. P. Jin

Received: 2 September 2010 / Accepted: 24 November 2010 / Published online: 16 December 2010  
© Springer Science+Business Media, LLC 2010

**Abstract** Based on the assessed three constituent binary systems and reported phase diagram data, the Co–Al–W ternary system was thermodynamically optimized by using CALculation PHAse Diagram (CALPHAD) method. The newly reported ternary phase  $\gamma'$  was described with a two sublattice model,  $(\text{Co},\text{Al},\text{W})_{0.75}:(\text{Co},\text{Al},\text{W})_{0.25}$ , while liquid Fcc, Hcp(Co), and Bcc(W) were treated as substitutional solution phases. In order to describe the ternary solubility in the binary phases  $\text{Co}_7\text{W}_6$  and  $\text{CoAl}$ , the models  $(\text{Al},\text{Co},\text{W})_7\text{W}_2(\text{Al},\text{Co},\text{W})_4$  and  $(\text{Al},\text{Co},\text{W})_{0.5}(\text{Al},\text{Co},\text{W})_{0.5}(\text{Va})_3$  were, respectively, adopted. The rest 11 phases in the ternary systems were simply treated as stoichiometric compounds because their homogeneous ranges are small and can be neglected. A set of self-consistent parameters were obtained, which reasonably reproduced the phase relationship in Co-enriched corner. Finally, to confirm the reliability of the present assessment, the so-called Scheil–Gulliver model was used to simulate the solidification processes of three typical Co-based alloys. It was shown that the as-cast microstructures of the three ingots were well explained or predicted.

## Introduction

Compared with Ni-based superalloys, Co-based alloys exhibit better resistance of hot corrosion and oxidation, so they are regarded as promising candidates for application at high temperature [1]. However, Co-based alloys were not used as widely as Ni-based superalloys in the past because the high-temperature strength of Co-based alloys is inferior to that of Ni-based alloys. To improve the high-temperature performance of Co-based alloys attracts much attention from researchers. It is well known that Ni-based superalloys are strengthened by  $\gamma'$  precipitated in the disordered fcc matrix phase ( $\gamma$ ), and  $\gamma'$  is a  $\text{L}1_2$ -ordered phase of  $\text{Ni}_3\text{Al}$  with ternary solubility. This guides researchers to find geometrically close-packed phases which possess the formula  $\text{A}_3\text{B}$  like  $\text{Ni}_3\text{Al}$  in Co-based alloys. Although  $\text{Co}_3\text{Ti}$  and  $\text{Co}_3\text{Ta}$  have been reported,  $\text{Co}_3\text{Ti}$  of  $\text{L}1_2$  structure could only be applied to temperatures below 750 °C and ordered face-centered cubic  $\text{Co}_3\text{Ta}$  was metastable and ready to convert to hexagonal closed-packed structure [2–5]. The development of Co-based alloys seems to be immersed in bottleneck.

Recently, this situation has been changed because of a new discovery of stable  $\text{L}1_2$ -ordered  $\text{Co}_3(\text{Al},\text{W})$  [6]. This finding stimulates interest to develop a new generation of Co-based alloys. Microstructures, physical and mechanical properties of alloys with  $\gamma/\gamma'$  duplex microstructure and  $\gamma'$  single-phase alloys have been investigated [7–13]. Both experiments [10] and calculations [13] indicated that the ductility of  $\text{Co}_3(\text{Al},\text{W})$  was expected to be sufficiently high so that  $\text{Co}_3(\text{Al},\text{W})$  can be practically used as the strengthening phase of Co-base superalloys.

Phase diagrams and thermodynamic properties of Co–Al–W alloys can help to design reasonable composition and heat treatment, thus they are important to develop

Y. F. Cui · X. Zhang · G. L. Xu · W. J. Zhu ·  
H. S. Liu (✉) · Z. P. Jin  
School of Materials Science and Engineering,  
Central South University, Changsha, Hunan 410083,  
People's Republic of China  
e-mail: hsliu@mail.csu.edu.cn

H. S. Liu · Z. P. Jin  
Center of Phase Diagrams and Materials Design,  
Central South University, Changsha, Hunan 410083,  
People's Republic of China

Co-based alloys. In this study, the Co–Al–W ternary system is thermodynamically assessed based on the constituent binaries and ternary experimental data reported [6] by using CALculation PHAse Diagram (CALPHAD) method. This approach employs collected experimental data to obtain a reliable assessment of properties and phase diagrams. Then solidification processes of typical alloys are simulated and compared with experimental observations.

## Evaluation of the available information

### Constituent binary systems

The Co–Al system was assessed first by Dupin and Ansara [14] and later by Ohtani et al. [15, 16]. The parameters obtained by Dupin and Ansara [14] may lead to unreasonable stability of Co–Al at high temperature. In the study of Ohtani et al. [15], the CsCl-type compound, Co–Al, was described with four-sublattice model. Later, Ohtani et al. adopted a two-sublattice model to optimize Co–Al [16]. For simplicity, thermodynamic parameters in Ref. [16] were used. In addition, Ohtani et al. [16] did not confirm the phase separation of ferromagnetic  $\alpha$ -Co and paramagnetic  $\alpha$ -Co while thermodynamic parameters of Co–W taken in this study considered this matter. In order to unify the description of Fcc(Co) and Hcp(Co), thermodynamic parameters treating contribution from magnetic transformation of the two phases in Ref. [16] will be slightly modified.

Thermodynamic optimization of Co–W system was first performed by Kaufman and Nesor [17] based on the subregular solution approximation. Then Gabriel et al. [18] reassessed this system considering new experimental results. But in the later description [18],  $\text{Co}_7\text{W}_6$  ( $\mu$  phase) was treated as a stoichiometric compound and the magnetic contribution to the Gibbs energy was not included. Taking into account the magnetic contribution and solubility range of  $\text{Co}_7\text{W}_6$ , Guillermet [19] reassessed the Co–W system. More recently, Sato et al. [20] applied a more reasonable model to describe  $\text{Co}_7\text{W}_6$  to fit the solubility range. In the study, thermodynamic parameters for the Co–W system were taken from Sato et al. [20].

Thermodynamic description of the Al–W system was recently performed in the frame of the COST 507 project [21], which will be directly adopted in this study.

### Co–Al–W ternary system

Two isothermal sections of the Co–Al–W ternary system in Co-rich corner at 1173 K and 1273 K were constructed by Sato et al. [6]. It was found that  $\gamma'$  was stable at 1173 K but metastable at 1273 K. This point of view was inconsistent

with Kobayashi et al. [22]. In the study of Kobayashi et al. [22], phase relations in the Co-rich corner at 1173 K were re-examined using diffusion-couple method, and  $\gamma'$  was regarded to be metastable at 1173 K. However, according to the DSC measurement, the solvus temperature of  $\gamma'$  was about 1263 K [6], and  $\gamma'$  did appear as a reaction product at the interface in the studied Co–27Al/Co–15 W couple at 1173 K [22]. Although the stable temperature range of  $\gamma'$  in the Co–Al–W system is not well confirmed,  $\gamma'$  should be stable in the temperature range from 1173 to 1263 K.

### Thermodynamic models

Different models are employed to describe the solution phases and intermetallic compounds in the Co–Al–W ternary system.

The solution phases: liquid, Fcc(Co), Hcp(Co), Fcc(Al), and Bcc(W)

The liquid is modeled as a substitutional solution phase and its Gibbs energy is described by the following formula:

$$G_m^L = \sum_{i=\text{Co,Al,W}} x_i^0 G_i^L + RT \sum_{i=\text{Co,Al,W}} x_i \ln x_i + E G_m^L \quad (1)$$

where  $G_m^L$  is the molar Gibbs energy of the liquid phase,  $x_i^0 G_i^L$  the Gibbs energy of pure element  $i$  ( $i = \text{Co, Al, W}$ ) in the structural state of liquid,  $R$  is the gas constant, and  $T$  is the temperature. And the excess Gibbs energy,  $E G_m^L$ , can be expressed by Redlich–Kister polynomial function as follows:

$$\begin{aligned} E G_m^L = & x_{\text{Co}} x_{\text{Al}} \sum_{j=0,1,\dots}^n {}^{(j)} L_{\text{Co,Al}}^L (x_{\text{Co}} - x_{\text{Al}})^j \\ & + x_{\text{Al}} x_{\text{W}} \sum_{j=0,1,\dots}^n {}^{(j)} L_{\text{Al,W}}^L (x_{\text{Al}} - x_{\text{W}})^j \\ & + x_{\text{Co}} x_{\text{W}} \sum_{j=0,1,\dots}^n {}^{(j)} L_{\text{Co,W}}^L (x_{\text{Co}} - x_{\text{W}})^j \\ & + x_{\text{Al}} x_{\text{Co}} x_{\text{W}} L_{\text{Al,Co,W}}^L \end{aligned} \quad (2)$$

here  $x_{\text{Co}}$ ,  $x_{\text{Al}}$ , and  $x_{\text{W}}$  are the mole fractions of component Co, Al, and W, respectively. The binary atomic interaction,  ${}^{(j)} L_{\text{Co,Al}}^L$ ,  ${}^{(j)} L_{\text{Al,W}}^L$ , and  ${}^{(j)} L_{\text{Co,W}}^L$  are, respectively, taken from Ohtani et al. [16], COST 507 [21] and Sato et al. [20].

Gibbs energy of Fcc(Co), Hcp(Co), and Bcc(W) is, respectively, described by splitting it into a nonmagnetic contribution ( ${}^{\text{nmag}} G$ ) and a magnetic term ( ${}^{\text{mag}} G$ ). The nonmagnetic part  ${}^{\text{nmag}} G$  is given by an equation similar to Eq. 1, and the magnetic part  ${}^{\text{mag}} G$  is described according to Hillert and Jarl [23] as:

$${}^{\text{mag}}G_{\text{m}}^i = RT \ln(\beta^i + 1) * f(\tau) \quad (3)$$

$$\begin{aligned} f(\tau) &= 1 - \left[ \frac{79\tau^{-1}}{140p} + \frac{474}{497} \left( \frac{1}{p} - 1 \right) \right. \\ &\quad \times \left. \left( \frac{\tau^3}{6} + \frac{\tau^9}{135} + \frac{\tau^{15}}{600} \right) \right] / A \quad \text{for } \tau = \frac{T}{T_c} \leq 1 \\ &= - \left[ \left( \frac{\tau^{-5}}{10} + \frac{\tau^{-15}}{315} + \frac{\tau^{-25}}{1500} \right) \right] / A \quad \text{for } \tau = \frac{T}{T_c} \geq 1 \end{aligned} \quad (4)$$

$$A = \frac{518}{1125} + \frac{11692}{15975} \left( \frac{1}{p} - 1 \right) \quad (5)$$

where  $p$  is the constant given by 0.28 for fcc and hcp metals and 0.4 for bcc metals. And  $\beta^i$  is the Bohr magneton number,  $T_c$  is the Curie temperature for magnetic materials. Both are, respectively, formulated as functions of alloy composition

$$\begin{aligned} T_c^i &= {}^0T_{\text{c},\text{Co}}^i x_{\text{Co}}^i + {}^0T_{\text{c},\text{Al}}^i x_{\text{Al}}^i + {}^0T_{\text{c},\text{W}}^i x_{\text{W}}^i \\ &+ \sum_{m=0,1,\dots}^n {}^mT_{\text{c},\text{CoW}}^i (x_{\text{Co}}^i - x_{\text{W}}^i) {}^m x_{\text{Co}}^i x_{\text{W}}^i \\ &+ \sum_{m=0,1,\dots}^n {}^mT_{\text{c},\text{CoAl}}^i (x_{\text{Co}}^i - x_{\text{Al}}^i) {}^m x_{\text{Co}}^i x_{\text{Al}}^i \\ &+ \sum_{m=0,1,\dots}^n {}^mT_{\text{c},\text{AlW}}^i (x_{\text{Al}}^i - x_{\text{W}}^i) {}^m x_{\text{Al}}^i x_{\text{W}}^i \\ &+ x_{\text{Co}}^i x_{\text{Al}}^i x_{\text{W}}^i T_{\text{c},\text{CoAlW}}^i \end{aligned} \quad (6)$$

and

$$\begin{aligned} \beta^i &= {}^0\beta_{\text{Co}}^i x_{\text{Co}}^i + {}^0\beta_{\text{Al}}^i x_{\text{Al}}^i + {}^0\beta_{\text{W}}^i x_{\text{W}}^i \\ &+ \sum_{m=0,1,\dots}^n {}^m\beta_{\text{Co,W}}^i (x_{\text{Co}}^i - x_{\text{W}}^i) {}^m x_{\text{Co}}^i x_{\text{W}}^i \\ &+ \sum_{m=0,1,\dots}^n {}^m\beta_{\text{Co,Al}}^i (x_{\text{Co}}^i - x_{\text{Al}}^i) {}^m x_{\text{Co}}^i x_{\text{Al}}^i \\ &+ \sum_{m=0,1,\dots}^n {}^m\beta_{\text{Al,W}}^i (x_{\text{Al}}^i - x_{\text{W}}^i) {}^m x_{\text{Al}}^i x_{\text{W}}^i \\ &+ x_{\text{Co}}^i x_{\text{Al}}^i x_{\text{W}}^i \beta_{\text{Co,Al,W}}^i \end{aligned} \quad (7)$$

here  ${}^0T_{\text{c},\text{Co}}^i$ ,  ${}^0T_{\text{c},\text{Al}}^i$ , and  ${}^0T_{\text{c},\text{W}}^i$  and  ${}^0\beta_{\text{Co}}^i$ ,  ${}^0\beta_{\text{Al}}^i$ , and  ${}^0\beta_{\text{W}}^i$  are magnetic transition temperature and Bohr number of pure Co, Al, and W, respectively.

### Ordered L1<sub>2</sub> phase ( $\gamma'$ )

The ordered L1<sub>2</sub> phase ( $\gamma'$ ) in the Co–Al–W system is modeled with a two-sublattice model, (Co,Al,W)<sub>0.75</sub>(Co,Al,W)<sub>0.25</sub>. In order to conveniently and simply describe the Gibbs energy of the ordered and the corresponding disordered phases in Al–Ni system, Ansara et al.

[24] derived an equation which allows thermodynamic properties of the disordered phase to be evaluated independently. In light of Ansara et al. [24], Gibbs energy of  $\gamma'$  phase is given as

$$\begin{aligned} G_{\text{m}}^{\text{Fcc},\text{L1}_2} &= G_{\text{m}}^{\text{Fcc}}(x_{\text{Co}}, x_{\text{Al}}, x_{\text{W}}) \\ &+ G_{\text{m}}^{\text{L1}_2}(y_{\text{Co}}^{\parallel}, y_{\text{Al}}^{\parallel}, y_{\text{W}}^{\parallel}, y_{\text{Co}}^{\parallel\parallel}, y_{\text{Al}}^{\parallel\parallel}, y_{\text{W}}^{\parallel\parallel}) \\ &- G_{\text{m}}^{\text{L1}_2}(x_{\text{Co}}, x_{\text{Al}}, x_{\text{W}}) \end{aligned} \quad (8)$$

where  $y_{\text{Co}}^{\parallel}$ ,  $y_{\text{Al}}^{\parallel}$  and  $y_{\text{W}}^{\parallel}$  are the site fractions of Co, Al, and W in the first sublattice, and  $y_{\text{Co}}^{\parallel\parallel}$ ,  $y_{\text{Al}}^{\parallel\parallel}$ ,  $y_{\text{W}}^{\parallel\parallel}$ , in the second one. On the right side of Eq. 8 and  $G_{\text{m}}^{\text{Fcc}}(x_{\text{Co}}, x_{\text{Al}}, x_{\text{W}})$  is the Gibbs energy of the disordered fcc phase.  $G_{\text{m}}^{\text{L1}_2}(y_{\text{Co}}^{\parallel}, y_{\text{Al}}^{\parallel}, y_{\text{W}}^{\parallel}, y_{\text{Co}}^{\parallel\parallel}, y_{\text{Al}}^{\parallel\parallel}, y_{\text{W}}^{\parallel\parallel})$  can be formulated from the corresponding sublattice model and implicitly contains a contribution from the disordered state. The last term,  $G_{\text{m}}^{\text{L1}_2}(x_{\text{Co}}, x_{\text{Al}}, x_{\text{W}})$ , represents transformation energy from the disordered state to the ordered state. When the site fractions are equal, i.e.,  $y_{\text{Co}}^{\parallel} = y_{\text{Co}}^{\parallel\parallel}$ ,  $y_{\text{Al}}^{\parallel} = y_{\text{Al}}^{\parallel\parallel}$  and  $y_{\text{W}}^{\parallel} = y_{\text{W}}^{\parallel\parallel}$ , the last two terms cancel each other. In this case, Eq. 8 describes the disordered state. More details about the model can be found in Refs. [24, 25].

### Binary phases with ternary solubility

In the Co–Al–W system, Al can partially solve in the Co<sub>7</sub>W<sub>6</sub> ( $\mu$ ) phase though the real atomic occupation in this phase has not been determined. As atomic radius difference between Al and Co atoms is smaller than the difference between Al and W atoms, Al atoms may preferably substitute for Co atoms in the lattice. So (Al,Co,W)<sub>7</sub>W<sub>2</sub> (Al,Co,W)<sub>4</sub> is adopted to describe Co<sub>7</sub>W<sub>6</sub>. This model is a normal extension of the model used for the Co–W binary system [20]. Gibbs energy of  $\mu$  in the ternary system is expressed with:

$$\begin{aligned} G_{\text{m}}^{\text{Co}_7\text{W}_6} &= \sum_i \sum_j y_i^{\parallel} y_j^{\parallel\parallel} G_{i;W;j}^{\text{Co}_7\text{W}_6} \\ &+ 7RT(y_{\text{Co}}^{\parallel} \ln y_{\text{Co}}^{\parallel} + y_{\text{Al}}^{\parallel} \ln y_{\text{Al}}^{\parallel} + y_{\text{W}}^{\parallel} \ln y_{\text{W}}^{\parallel}) \\ &+ 4RT(y_{\text{Co}}^{\parallel\parallel} \ln y_{\text{Co}}^{\parallel\parallel} + y_{\text{Al}}^{\parallel\parallel} \ln y_{\text{Al}}^{\parallel\parallel} + y_{\text{W}}^{\parallel\parallel} \ln y_{\text{W}}^{\parallel\parallel}) \\ &+ \sum_l \sum_{i>l} \sum_j y_l^{\parallel} y_i^{\parallel} y_j^{\parallel\parallel} L_{l,i;W;j}^{\text{Co}_7\text{W}_6} \\ &+ \sum_l \sum_j \sum_{k>j} y_l^{\parallel} y_j^{\parallel} y_k^{\parallel\parallel} L_{l;W;j,k}^{\text{Co}_7\text{W}_6} \\ &+ \sum_l \sum_{i>l} \sum_{m>i} \sum_n y_l^{\parallel} y_i^{\parallel} y_m^{\parallel} y_n^{\parallel\parallel} L_{l,i,m;W;n}^{\text{Co}_7\text{W}_6} \\ &+ \sum_l \sum_j \sum_{k>j} \sum_{n>k} y_l^{\parallel} y_j^{\parallel} y_k^{\parallel} y_n^{\parallel\parallel} L_{l;W;j,k,n}^{\text{Co}_7\text{W}_6} \end{aligned} \quad (9)$$

here  $i$ ,  $l$ , and  $m$  denote Co, Al, W in the first sublattice and  $j$ ,  $k$ , and  $n$  indicate Co, Al, W in the third one, respectively.

$G_{i:W:j}^{Co_7W_6}$ ,  $L_{Co,W:W:j}^{Co_7W_6}$ ,  $L_{i:W:Co,W}^{Co_7W_6}$ , ( $i,j = \text{Co or W}$ ) are taken directly from Sato et al. [20]. Other parameters are to be optimized in this study.

For CoAl (Bcc\_B2) phase, a sublattice model,  $(\text{Al},\text{Co},\text{W})_{0.5}(\text{Al},\text{Co},\text{W})_{0.5}(\text{Va})_3$ , is adopted, consequently its Gibbs energy is formulated with following equation:

$$\begin{aligned} G_m^{\text{CoAl}} = & \sum_i \sum_j y_i^\parallel y_j^\parallel G_{i:j:\text{Va}}^{\text{CoAl}} \\ & + 0.5RT(y_{\text{Co}}^\parallel \ln y_{\text{Co}}^\parallel + y_{\text{Al}}^\parallel \ln y_{\text{Al}}^\parallel + y_{\text{W}}^\parallel \ln y_{\text{W}}^\parallel) \\ & + 0.5RT(y_{\text{Co}}^\parallel \ln y_{\text{Co}}^\parallel + y_{\text{Al}}^\parallel \ln y_{\text{Al}}^\parallel + y_{\text{W}}^\parallel \ln y_{\text{W}}^\parallel) \\ & + \sum_l \sum_{i>l} \sum_j y_i^\parallel y_j^\parallel L_{l:i:j:\text{Va}}^{\text{CoAl}} \\ & + \sum_l \sum_j \sum_{k>j} y_l^\parallel y_j^\parallel y_k^\parallel L_{l:j,k:\text{Va}}^{\text{CoAl}} \\ & + \sum_l \sum_{i>l} \sum_{m>i} \sum_n y_l^\parallel y_i^\parallel y_m^\parallel y_n^\parallel L_{l,i,m:n:\text{Va}}^{\text{CoAl}} \\ & + \sum_l \sum_j \sum_{k>j,n>k} y_l^\parallel y_j^\parallel y_k^\parallel y_n^\parallel L_{l:j,k,n:\text{Va}}^{\text{CoAl}} \end{aligned} \quad (10)$$

in which  $G_{i:j:\text{Va}}^{\text{CoAl}}$ ,  $L_{\text{Al},\text{Co},j:\text{Va}}^{\text{CoAl}}$ ,  $L_{i:\text{Al},\text{Co}:\text{Va}}^{\text{CoAl}}$ , ( $i,j = \text{Al or Co}$ ) are taken from Ohtani et al. [16].

Solubility of Al in  $\text{Co}_3\text{W}$  is so limited that it is neglected for simplicity. And heat capacity of  $\text{Co}_3\text{W}$  is not available. Hence, Gibbs energy of  $\text{Co}_3\text{W}$  can be expressed using the Kopp–Neumann rule:

$$G_m^{\text{Co}_3\text{W}} = 3G_{\text{Co}}^{\text{HCP}-A^3} + G_{\text{W}}^{\text{Bcc}-A^2} + A + B * T \quad (11)$$

here  $A$  and  $B$  are constants that are taken from Sato et al. [20].

There is no other equilibrium information except Co-rich corner, so the ternary solubility of other binary phases,  $\text{Al}_5\text{Co}_2$ ,  $\text{Al}_3\text{Co}$ ,  $\text{Al}_{13}\text{Co}_4$ ,  $\text{Al}_9\text{Co}_2$ ,  $\text{Al}_2\text{W}$ ,  $\text{Al}_4\text{W}$ ,  $\text{Al}_{12}\text{W}$ ,  $\text{Al}_5\text{W}$ ,  $\text{Al}_7\text{W}_3$ , and  $\text{Al}_{77}\text{W}_{23}$ , is not considered at present. Hence, Eq. 11 is also employed to describe Gibbs energy of these phases.

## Results and discussion

### Assessment of the Co–Al–W system

Besides two isothermal sections about the Co–Al–W system, there is little information including thermochemical and phase equilibrium data reported. For simplicity, the ternary interaction parameters of liquid Fcc, Hcp(Co), and Bcc(W) are assumed to be zero. Similarly, ternary interaction parameters in the sublattice of CoAl and  $\text{Co}_7\text{W}_6$  are set to be zero.

By adopting the reported thermodynamic parameters of three constituent binaries [16, 20, 21], and on the basis of reported phase relationship in Co-enriched corner [6], the

Co–Al–W ternary system was further assessed by using the Pandat software package [26]. After the experimental data on phase diagrams were input to the program, all of the unknown parameters were varied by trial and error method during the whole assessment until most experimental data were reproduced within the expected uncertainty limits. All of the parameters acquired in this study are listed in Table 1.

Comparisons between the experimental and the calculated isothermal sections in Co-rich portion at 1173 K and 1273 K are shown in Figs. 1 and 2, respectively. It can be seen that most of the phase relations have been well reproduced.

Certainly, there are some differences between the calculated isothermal sections and the experimental ones. For example, according to Ref. [6], the  $\text{Co}_3(\text{Al},\text{W})$  single-phase field is located around Co–9.5Al–12.5 W (at%). In the calculated isothermal section, the composition of  $\gamma'$  is about Co–8.5Al–11.1 W (at%), slightly deviating from the experimental results. If the experimental error is taken into account, the discrepancy could be accepted.

### As-cast microstructure, solidification path, and simulation

To further check the reasonableness of the present assessment, solidification paths of typical Co-rich alloys are further measured and simulated using the Scheil–Gulliver model [27, 28], which assumes perfect mixing in liquid and no solute back diffusion in solid. This model has been integrated in Scheil Solidification Simulation module of Pandat software [26]. Comparisons between the observation and simulation are given in the next paragraphs.

Three ternary alloys were prepared by non-consumable tungsten electrode arc melting in a water-cooled copper crucible under argon atmosphere. High purity metals: 99.9% Co sheets, 99.99% Al grains, and 99.9% W grains were used as starting materials. Each sample was melted for at least three times to obtain homogenous distribution of composition. Microstructure of each sample was examined using scanning electron microscope (SEM), and phase composition was determined by energy-dispersive X-ray analysis (EDX). X-ray diffraction (XRD) was also performed to further identify the phases in the samples.

### Alloy 1 (55Co–10Al–35W, at%)

Figure 3 shows XRD pattern of alloy 1. There are four phases in the as-cast alloy 1: Bcc(W),  $\text{Co}_7\text{W}_6$ , Fcc(Co), and AlCo. According to the rule of phase equilibrium, three phases at most can co-exist in an equilibrated ternary alloy when temperature and pressure are kept constant. Thus at least one phase should be unstable in the as-cast state.

**Table 1** Thermodynamic parameters of Co–Al–W ternary system obtained in this work

Phase	Thermodynamic parameters	References
Liquid model: (Co,Al,W) <sub>1</sub>	$(^0)L_{\text{Co,Al}}^{\text{Liq}} = -157700 + 30.4 * T$ $(^1)L_{\text{Co,Al}}^{\text{Liq}} = -2600$ $(^2)L_{\text{Co,Al}}^{\text{Liq}} = 11600$ $(^3)L_{\text{Co,Al}}^{\text{Liq}} = 3250 + 1.735 * T$ $(^0)L_{\text{Al,W}}^{\text{Liq}} = -70000 + 35 * T$ $(^1)L_{\text{Al,W}}^{\text{Liq}} = 1E - 04$ $(^2)L_{\text{Al,W}}^{\text{Liq}} = 15000$ $(^0)L_{\text{Co,W}}^{\text{Liq}} = -18385.568 + 2.5858 * T$ $(^1)L_{\text{Co,W}}^{\text{Liq}} = -25165.674 + 3.8756 * T$ $(^2)L_{\text{Co,W}}^{\text{Liq}} = 41820.097 - 12.8623 * T$	[16] [16] [16] [16] [21] [21] [21] [20] [20] [20]
FCC_A1 Model:(Co,Al,W) <sub>1</sub> :(Va) <sub>1</sub>	$(^0)L_{\text{Co,Al}}^{\text{FCC}} = -105000$ $(^0)T_{\text{cCo,Al}}^{\text{Fcc}} = -3830$ $(^1)T_{\text{cCo,Al}}^{\text{Fcc}} = 970$ $(^0)\beta_{\text{Co,Al}}^{\text{Fcc}} = 10$ $(^0)L_{\text{Al,W}}^{\text{FCC}} = -19250 + 20.2 * T$ $(^1)L_{\text{Al,W}}^{\text{FCC}} = -10000$ $(^0)L_{\text{Co,W}}^{\text{FCC}} = -15626.162 + 8.1126 * T$ $(^1)L_{\text{Co,W}}^{\text{FCC}} = 1571.6936 - 5.9654 * T$ $(^2)L_{\text{Co,W}}^{\text{FCC}} = -9909.8886 + 3.1244 * T$ $(^0)T_{\text{cCo,W}}^{\text{Fcc}} = -3520.31$ $(^1)T_{\text{cCo,W}}^{\text{Fcc}} = -4796.2$ $(^2)T_{\text{cCo,W}}^{\text{Fcc}} = -813.657$ $(^3)T_{\text{cCo,W}}^{\text{Fcc}} = 5699.827$ $(^0)\beta_{\text{Co,W}}^{\text{Fcc}} = -2.92662$ $(^1)\beta_{\text{Co,W}}^{\text{Fcc}} = -4.76958$ $(^2)\beta_{\text{Co,W}}^{\text{Fcc}} = -4.54864$ $(^3)\beta_{\text{Co,W}}^{\text{Fcc}} = 10.14396$	[16] This work This work This work [21] [21] [20] [20] [20] [20] [20] [20] [20] [20] [20] [20] [20] [20] [20]
HCP_A3 Model: (Co,Al,W) <sub>1</sub> (Va) <sub>0.5</sub>	$G_{\text{Al}}^{\text{HCP}} = 5481 - 1.799 * T + \text{GHSERAL}$ $G_{\text{W}}^{\text{HCP}} = 14750 + \text{GHSERW}$ $(^0)T_{\text{cAI,Co}}^{\text{HCP}} = -1830$ $(^1)T_{\text{cAI,Co}}^{\text{HCP}} = 970$ $(^0)\beta_{\text{Al,Co}}^{\text{HCP}} = 10$ $(^0)L_{\text{Co,W}}^{\text{HCP}} = -17817.537 + 12.4569 * T$ $(^1)L_{\text{Co,W}}^{\text{HCP}} = 5639.8548 - 9.5239 * T$ $(^2)L_{\text{Co,W}}^{\text{HCP}} = -2285.7125 - 1.4073 * T$ $(^0)T_{\text{cCo,W}}^{\text{HCP}} = -3159.19$ $(^1)T_{\text{cCo,W}}^{\text{HCP}} = -4023.37$ $(^2)T_{\text{cCo,W}}^{\text{HCP}} = 200.523$ $(^3)T_{\text{cCo,W}}^{\text{HCP}} = 5538.65$ $(^0)\beta_{\text{Co,W}}^{\text{HCP}} = -2.92662$ $(^1)\beta_{\text{Co,W}}^{\text{HCP}} = -4.76958$ $(^2)\beta_{\text{Co,W}}^{\text{HCP}} = -4.54864$ $(^3)\beta_{\text{Co,W}}^{\text{HCP}} = 10.14396$	[16] [20] This work This work This work [20] [20] [20] [20] [20] [20] [20] [20] [20] [20] [20] [20] [20]

**Table 1** continued

**Table 1** continued

Phase	Thermodynamic parameters	References
	$G_{\text{Al:Co}}^{L1_2} = G_{\text{Co:Al}}^{L1_2} = 3 * \text{U}_{\text{ALCo}}; G_{\text{Al:W}}^{L1_2} = G_{\text{W:Al}}^{L1_2} = 3 * \text{U}_{\text{ALW}}$ ;	This work
	$G_{\text{Co:W}}^{L1_2} = G_{\text{W:Co}}^{L1_2} = 3 * \text{U}_{\text{CoW}}$ ;	
	$L_{\text{Al:Co:Co}}^{L1_2} = L_{\text{Al:Co:W}}^{L1_2} = L_{\text{Al:Co:Al}}^{L1_2} = 6 * \text{U}_{\text{AlCo}}$ ;	This work
	$L_{\text{Co,W:Al}}^{L1_2} = L_{\text{Co,W:Co}}^{L1_2} = L_{\text{Co,W:W}}^{L1_2} = 6 * \text{U}_{\text{CoW}}$ ;	
	$L_{\text{Al,W:Co}}^{L1_2} = L_{\text{Al,W:Al}}^{L1_2} = L_{\text{Al,W:W}}^{L1_2} = 6 * \text{U}_{\text{AlW}}$ ;	
	$L_{\text{Al:Al,Co}}^{L1_2} = L_{\text{Co:Al,Co}}^{L1_2} = L_{\text{W:Al,Co}}^{L1_2} = 0$ ;	This work
	$L_{\text{Al:Co,W}}^{L1_2} = L_{\text{Co:Co,W}}^{L1_2} = L_{\text{W:Co,W}}^{L1_2} = 0$ ;	
	$L_{\text{Al:Al,W}}^{L1_2} = L_{\text{Co:Al,W}}^{L1_2} = L_{\text{W:Al,W}}^{L1_2} = 0$ ;	
Co <sub>3</sub> W Model: (Co) <sub>3</sub> :(W) <sub>1</sub>	$G_{\text{Co,W}}^{\text{Co,W}} = -31976.631 + 10.9409 * T + 3 * \text{GHSERCO} + \text{GHSERW}$	[20]
Al <sub>5</sub> Co <sub>2</sub> Model: (Al) <sub>0.714</sub> :(Co) <sub>0.286</sub>	$G_{\text{Al:Co}}^{\text{Al}_5\text{Co}_2} = -47000 + 8.914 * T + 0.714 * \text{GHSERAL}$ + 0.286 * GHSERCO	[16]
Al <sub>3</sub> Co Model: (Al) <sub>0.75</sub> :(Co) <sub>0.25</sub>	$G_{\text{Al:Co}}^{\text{Al}_3\text{Co}} = -42500 + 7.78 * +5.14E - 04 * T * \text{LN}(T)$ + 0.75 * GHSERAL + 0.25 * GHSERCO	[16]
Al <sub>13</sub> Co <sub>4</sub> Model: (Al) <sub>0.765</sub> :(Co) <sub>0.235</sub>	$G_{\text{Al:Co}}^{\text{Al}_{13}\text{Co}_4} = -40200 + 7.1 * T + 0.765 * \text{GHSERAL}$ + 0.235 * GHSERCO	[16]
Al <sub>9</sub> Co <sub>2</sub> Model: (Al) <sub>0.818</sub> :(Co) <sub>0.182</sub>	$G_{\text{Al:Co}}^{\text{Al}_9\text{Co}_2} = -32100 + 5.346 * T + 9.4E - 04 * T * \text{LN}(T)$ + 0.818 * GHSERAL + 0.182 * GHSERCO	[16]
Al <sub>2</sub> W Model: (Al) <sub>2</sub> :(W) <sub>1</sub>	$G_{\text{Al:W}}^{\text{Al}_2\text{W}} = 13536 - 22.38 * T + 2 * \text{GHSERAL} + \text{GHSERW}$	[21]
Al <sub>4</sub> W Model: (Al) <sub>4</sub> :(W) <sub>1</sub>	$G_{\text{Al:W}}^{\text{Al}_4\text{W}} = -57500 + 9.73 * T + 4 * \text{GHSERAL} + \text{GHSERW}$	[21]
Al <sub>12</sub> W Model: (Al) <sub>12</sub> :(W) <sub>1</sub>	$G_{\text{Al:W}}^{\text{Al}_{12}\text{W}} = -62400 + 9.49 * T + 12 * \text{GHSERAL} + \text{GHSERW}$	[21]
Al <sub>5</sub> W Model: (Al) <sub>5</sub> :(W) <sub>1</sub>	$G_{\text{Al:W}}^{\text{Al}_5\text{W}} = -58446 + 8.4 * T + 5 * \text{GHSERAL} + \text{GHSERW}$	[21]
Al <sub>7</sub> W <sub>3</sub> Model: (Al) <sub>7</sub> :(W) <sub>3</sub>	$G_{\text{Al:W}}^{\text{Al}_7\text{W}_3} = 34700 - 70 * T + 7 * \text{GHSERAL} + 3 * \text{GHSERW}$	[21]
Al <sub>77</sub> W <sub>23</sub> Model: (Al) <sub>77</sub> :(W) <sub>23</sub>	$G_{\text{Al:W}}^{\text{Al}_{77}\text{W}_{23}} = -189300 - 400 * T + 77 * \text{GHSERAL} + 23 * \text{GHSERW}$	[21]

Back-scattered Electronic (BSE) image of the as-cast microstructure of alloy 1 is illustrated in Fig. 4. As seen, four phases of various shapes exist in the alloy. According to EDX result, the white phase corresponds to Bcc(W), white-gray to Co<sub>7</sub>W<sub>6</sub>, gray to Fcc(Co), and dark to AlCo. The Bcc(W) is of coarse dendritic morphology and closely wrapped by Co<sub>7</sub>W<sub>6</sub> (Fig. 4). This indicates the feature of primary solidification product. The wrapping Co<sub>7</sub>W<sub>6</sub> should be the product of a binary peritectic reaction involving Bcc(W). Besides, the binary or ternary eutectic structure involving Fcc(Co) and AlCo is also apparent.

Liquidus projection of the Co-Al-W system together with solidification path for the alloy 1 is calculated as illustrated in Fig. 5. In light of the present calculation, Bcc(W) will first crystallize from liquid phase, then Co<sub>7</sub>W<sub>6</sub>, Fcc(Co), and AlCo will form through the following reactions in sequence: Liquid + Bcc(W) → Co<sub>7</sub>W<sub>6</sub>, Liquid → Co<sub>7</sub>W<sub>6</sub>, Liquid → Co<sub>7</sub>W<sub>6</sub> + Fcc(Co), and Liquid → Co<sub>7</sub>W<sub>6</sub> + AlCo + Fcc(Co). However, during art-melting the cooling rate is so fast and it is difficult for W to diffuse through the wrapping Co<sub>7</sub>W<sub>6</sub>. Thus, the peritectic reaction, Liquid + Bcc(W) → Co<sub>7</sub>W<sub>6</sub>, has no sufficient time to proceed. Consequently, Bcc(W) remain in the ingot as the unstable phase and partial

liquid will directly transform to Co<sub>7</sub>W<sub>6</sub>. That means that Bcc(W), Co<sub>7</sub>W<sub>6</sub>, AlCo, and Fcc(Co) will co-exist in alloy 1. Evidently, this is in consistence with the observations. Besides, the eutectic structure in Fig. 4 is corresponding to the products through binary eutectic reaction Liquid → Co<sub>7</sub>W<sub>6</sub> + Fcc(Co) and ternary eutectic reaction Liquid → Co<sub>7</sub>W<sub>6</sub> + AlCo + Fcc(Co).

#### Alloy 2 (55Co–15Al–30W, at%)

The simulated solidification path of alloy 2 is shown in Fig. 6. It can be known, Bcc(W) will precipitate first from liquid. Then Co<sub>7</sub>W<sub>6</sub> will be produced through the following two reactions, Liquid + Bcc(W) → Co<sub>7</sub>W<sub>6</sub> and Liquid → Co<sub>7</sub>W<sub>6</sub>. Next, two eutectic reactions: Liquid → Co<sub>7</sub>W<sub>6</sub> + AlCo and Liquid → Co<sub>7</sub>W<sub>6</sub> + AlCo + Fcc(Co) will happen in turn. If equilibrium is reached, three phases (Co<sub>7</sub>W<sub>6</sub>, AlCo, and Fcc(Co)) at most will co-exist in alloy 2. However, during cooling in water-cooled copper crucible, the peritectic reaction, Liquid + Bcc(W) → Co<sub>7</sub>W<sub>6</sub>, was not completed. This leads unreacted Bcc(W) to be remained like in alloy 1. Hence, Bcc(W), Co<sub>7</sub>W<sub>6</sub>, AlCo, and Fcc(Co) are expected to co-exist in alloy 2. Both peritectic and

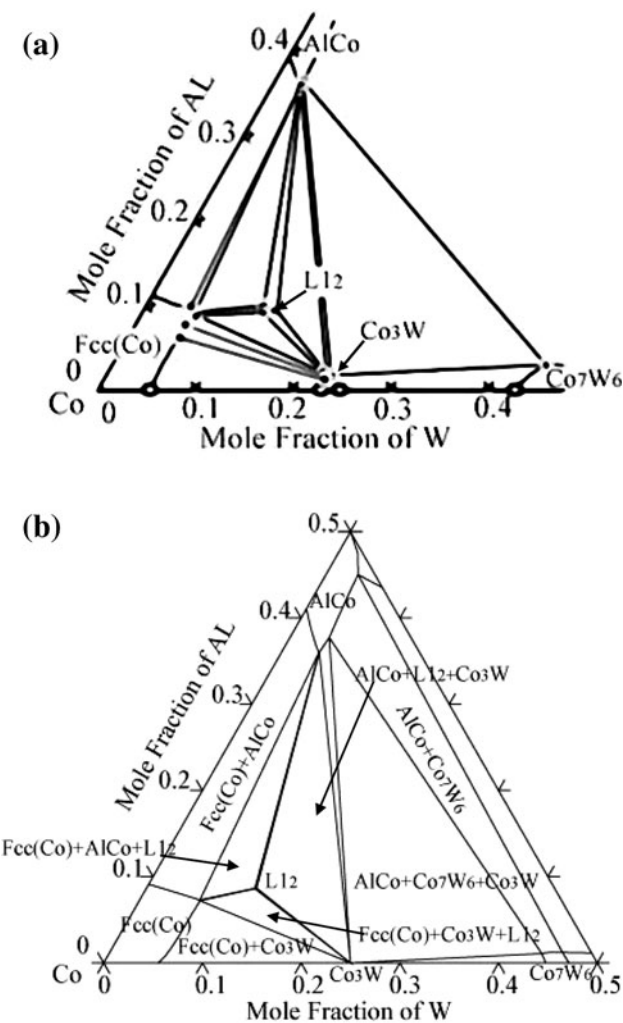


**Fig. 1** The isothermal section of Co–Al–W ternary system at 1173 K  
(a) measured by Sato et al. [6], (b) calculated in this study

eutectic structures should be observed in the microstructure image.

Experimental results are analyzed to verify these predictions. Figure 7 illustrates the microstructure image of alloy 2, which clearly contains primary and eutectic structure. The same four phases as in the calculation, Bcc(W), Co<sub>7</sub>W<sub>6</sub>, AlCo, and Fcc(Co), are confirmed. Also in Fig. 7, it can be clearly seen that Bcc(W) is wrapped by a thin layer of Co<sub>7</sub>W<sub>6</sub>. Like in alloy 1, such morphology feature corresponds to the peritectic reaction, Liquid + Bcc(W) → Co<sub>7</sub>W<sub>6</sub>. Besides, there are Co<sub>7</sub>W<sub>6</sub> of other different morphologies, including the part formed along AlCo and the other part, being of lamellar shape and distributing between the peritectic structure and AlCo. Correspondingly, they should be formed, respectively, through binary and ternary eutectic reaction, Liquid → Co<sub>7</sub>W<sub>6</sub> + AlCo and Liquid → Co<sub>7</sub>W<sub>6</sub> + AlCo + Fcc(Co). This obviously confirms the present calculation.

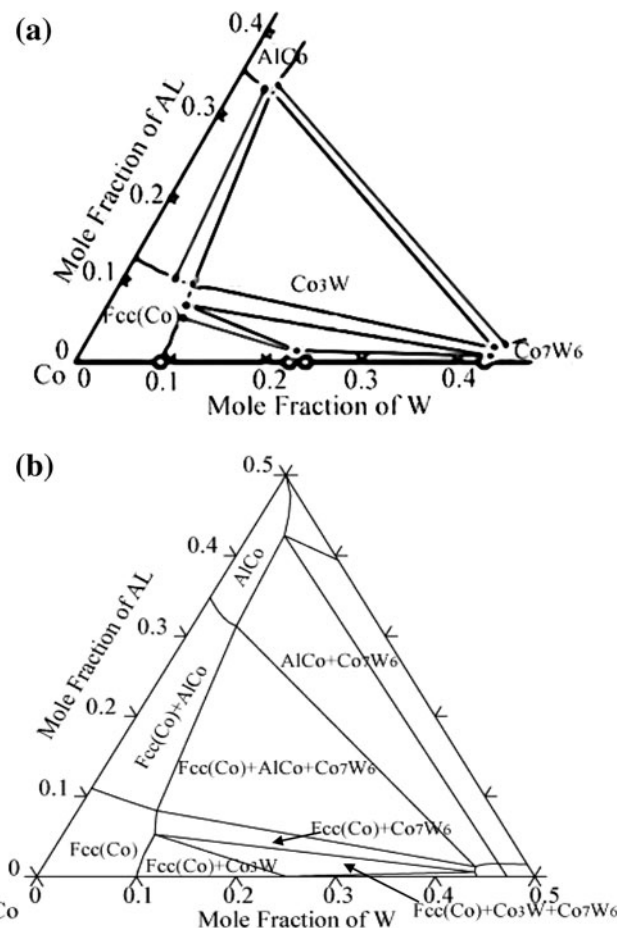


**Fig. 2** The isothermal section of Co–Al–W ternary system at 1273 K  
(a) measured by Sato et al. [6], (b) calculated in this study

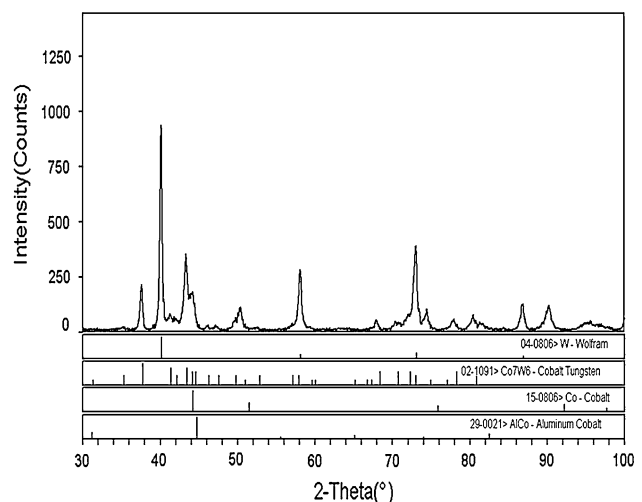


**Fig. 3** XRD patterns of as-cast alloy 1

Moreover, comparing alloy 2 with alloy 1, it is evident that the precipitation sequence and morphology of solid phases in these two alloys are distinct although they are

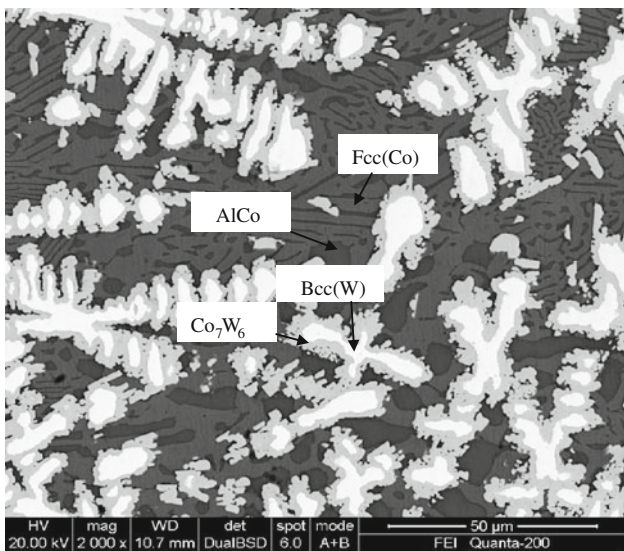


**Fig. 4** Back-scattered electron images of solidification microstructure for alloy 1

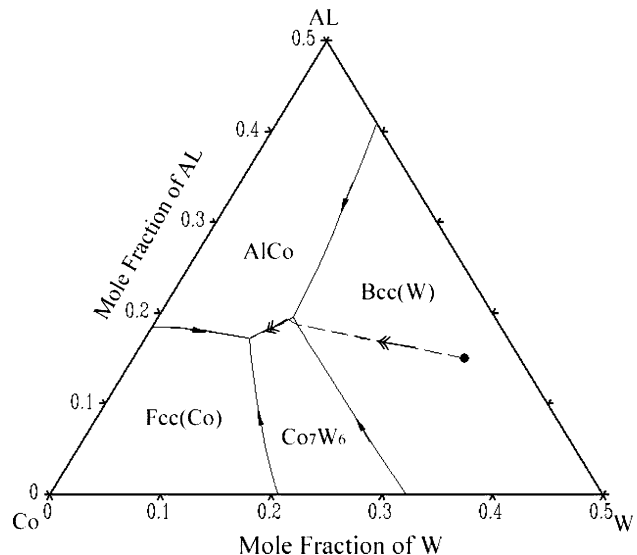


**Fig. 6** Calculated liquidus projection superposed with the solidification path (dashed line with  $\rightarrow$ ) for alloy 2

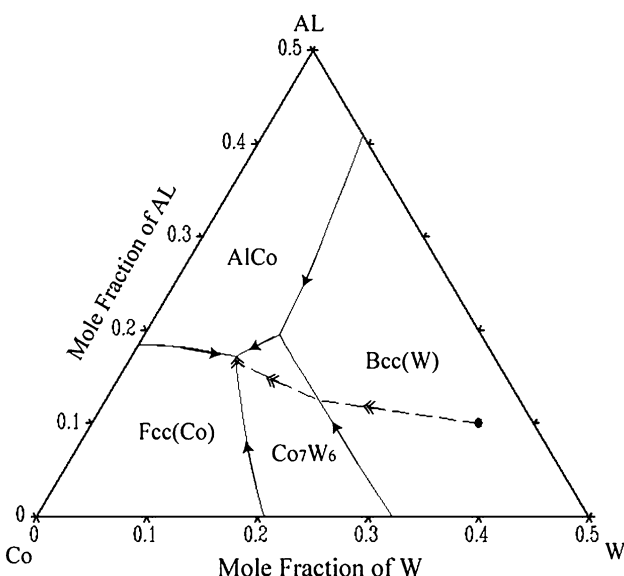


**Fig. 5** Calculated liquidus projection of the Co-Al-W ternary system superposed with the solidification path (dashed line with  $\rightarrow$ ) for alloy 1

composed of the same four phases. The different morphologies should result from different solidification paths.

#### Alloy 3 (76.4Co–16.3Al–7.3W, at%)

Solidification progress of alloy 3 is also simulated as shown in Fig. 8. Differing from alloys 1 and 2, Fcc(Co) will primarily crystallize from liquid phase. Next, AlCo will form through a binary eutectic reaction:

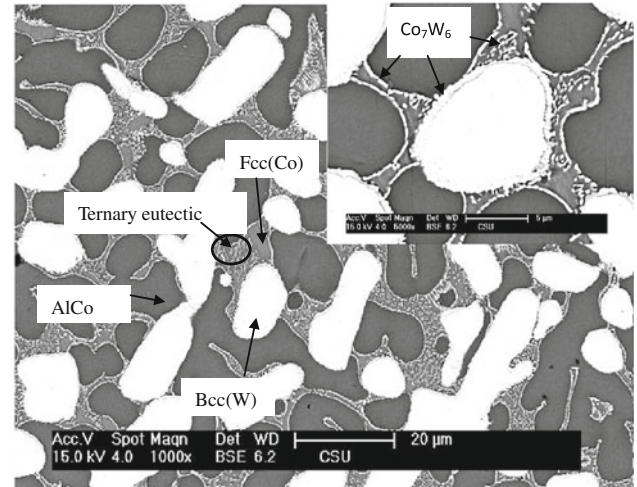


**Fig. 7** Back-scattered electron images of solidification microstructure for alloy 2

Liquid  $\rightarrow$  AlCo + Fcc(Co). Then the rest liquid will undergo a ternary eutectic reaction: Liquid  $\rightarrow$  Co7W6 + AlCo + Fcc(Co). If solidification is completed, three phases including Co7W6, AlCo, and Fcc(Co) will exist in alloy 3. However, as shown in Figs. 9 and 10, only AlCo (dark) and Fcc(Co) (white) are clearly observed by SEM-EDX and XRD pattern.

In order to explain the absence of Co7W6, mole fractions of solid phases are further calculated as illustrated in Fig. 11. In light of the calculation, mole fraction of Co7W6 is about 0.005, too low to be observed or detected. This could be the reason why Co7W6 should have formed but is not observed in Fig. 10. Besides, the typical coarse dendritic morphology of Fcc(Co) and eutectic structure

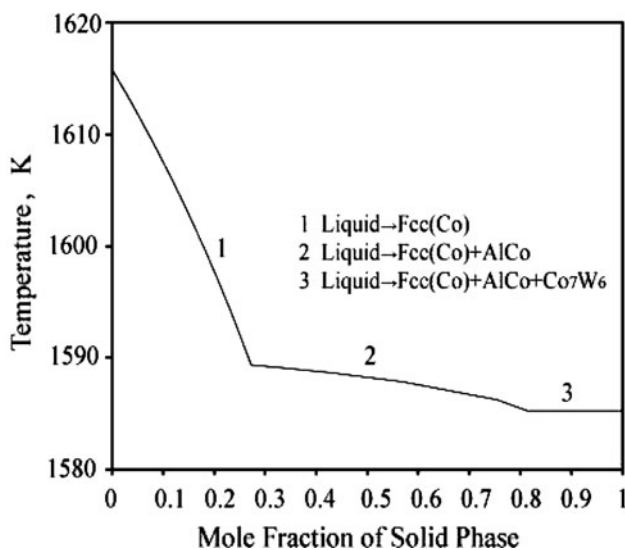


**Fig. 8** Calculated solidification processes for alloy 3

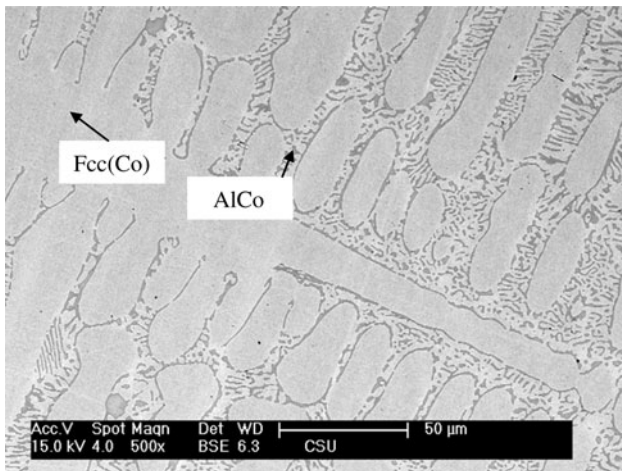


**Fig. 9** Back-scattered electron images of solidification microstructure for alloy 3

composed of Fcc(Co) and AlCo are observed in Fig. 9. These microstructures are, respectively, well consistent with the calculated solidification reactions: Liquid  $\rightarrow$  Fcc(Co), Liquid  $\rightarrow$  AlCo + Fcc(Co).

## Conclusions

First, based on the previous information about the ternary phase equilibrium, Co-Al-W system was thermodynamically described combining with the reported constituent binary systems. A set of self-consistent thermodynamic parameters have been constructed to reproduce the Co-Al-W ternary system. Then, with the Scheil-Gulliver model,

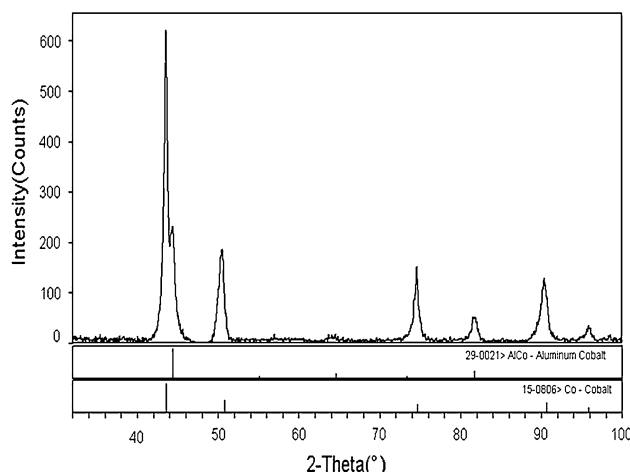


**Fig. 10** XRD patterns of as-cast alloy 3

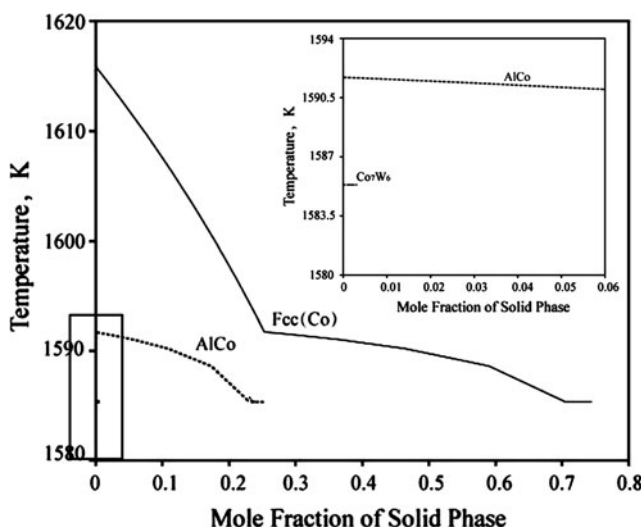


**Fig. 11** Calculated mole fractions of solid phase versus temperature for alloy 3

solidification paths of three typical Co-Al-W alloys were simulated using the present optimized parameters. The calculated solidification paths can reasonably explain the as-cast microstructures of various alloys.

**Acknowledgements** This study was financially supported by National Natural Science Foundation (Grant No. 50671122), P. R. China. Special acknowledgements are given to the Pandat program licensed from The CompuThermo, LLC, Madison, WI, USA.

## References

1. Beltran AM (1987) In: Sims CT, Stoloff NS, Hagel WC (eds) Superalloys II. Wiley, New York, p 135
2. Blaise JM, Viatour P, Drapier JM (1970) Cobalt 49:192
3. Viatour P, Drapier JM, Coutsouradis D (1973) Cobalt 3:67

4. Drapier JM, de JL Brouwer, Coutsouradis D (1965) Cobalt 27:59
5. Drapier JM, Coutsouradis D (1968) Cobalt 39:63
6. Sato J, Omori T, Oikawa K, Ohnuma I, Kainuma R, Ishida K (2006) Science 312:90
7. Suzuki A, Pollock TM (2008) Acta Mater 56:1288
8. Miura S, Ohkubo K, Mohri T (2007) Mater Trans 48:2403
9. Yao Q, Xing H, Sun J (2006) Appl Phys Lett 89:161906
10. Tanaka K, Ohashi T, Kishida K, Inui H (2007) Appl Phys Lett 91:181907
11. Inui H, Tanaka K, Kishida K, Okamoto NL, Oohashi T (2009) Mater Res Soc Symp Proc 1128:1128-U06-07
12. Oohashi T, Okamoto NL, Kishida K, Tanaka K, Inui H (2009) Mater Res Soc Symp Proc 1128:1128-U05-26
13. Jiang C (2008) Scripta Mater 59:1075
14. Dupin N, Ansara I (1998) Rev de Met 9:1121
15. Ohtani H, Chen Y, Hasebe M (2004) Mater Trans 45:1489
16. Ohtani H, Yamano M, Hasebe M (2004) CALPHAD 28:177
17. Kaufman L, Nesor H (1978) CALPHAD 2:81
18. Gabriel A, Lukas HL, Allibert CH, Ansara I (1985) Z Metallkd 76:589
19. Guillermet AF (1989) Metall Mater Trans A 20:935
20. Sato J, Oikawa K, Kainuma R, Ishida K (2005) Mater Trans 46:1199
21. Ansara I, Dinsdale AT, Rand MH (1998) COST 507 Thermochemical database for light metal alloys, Ver. 2
22. Kobayashi S, Tsukamoto Y, Takasugi T, Chinen H, Omori T, Ishida K, Zaeferer S (2009) Intermetallics 17:1085
23. Hillert M, Jarl M (1978) CALPHAD 2:227
24. Ansara I, Dupin N, Lukas HL, Sundman B (1997) J Alloy Compds 247:20
25. Huang W, Chang YA (1999) Intermetallics 7:863
26. PANDAT software for multicomponent phase diagram calculations by CompuTherm LLC, Madison, WI, 2000
27. Scheil E (1942) Z Metallkd 34:70
28. Gulliver JM (1913) J Inst Meteorol 9:120